## Supplemental Figures and Legends

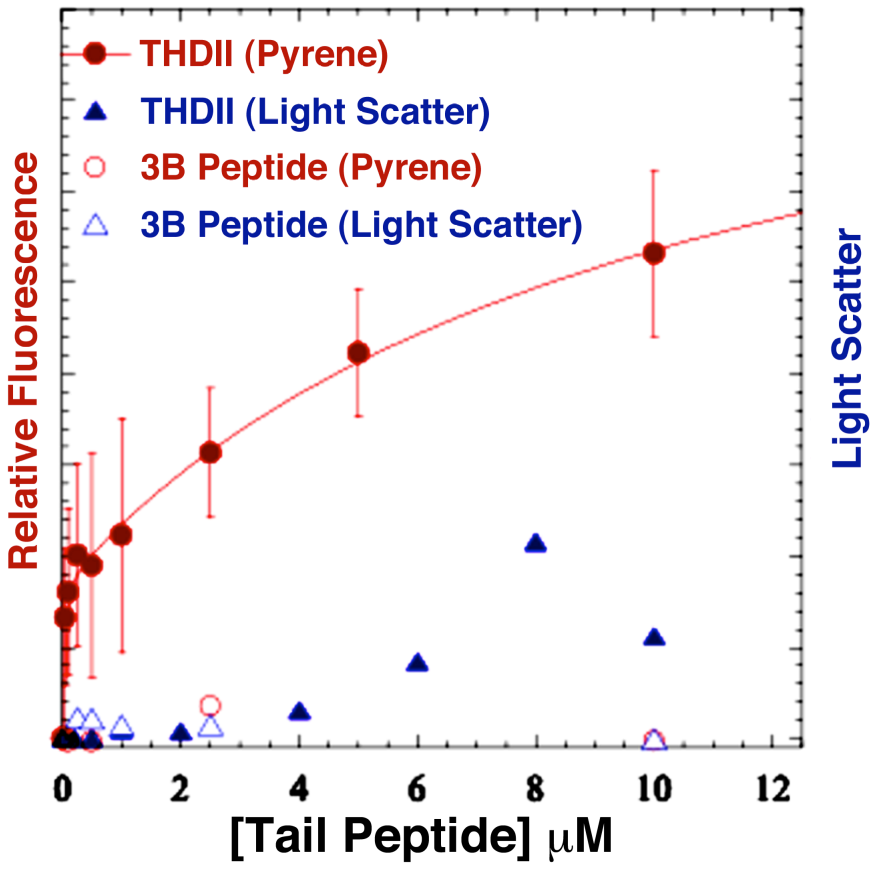


**Figure S1, related to Figure 1.** The tail fragment of MYO3A binds directly to actin. Our examination of the degree of pyrene actin (0.2 μM) fluorescence quenching as a function of THDII peptide was found to contain two components. Light scatter was also used to monitor the degree of actin bundling, which demonstrated that bundling does not occur until peptide concentrations are greater than 2 μM. There was no pyrene quenching or change in light scatter observed with a peptide derived from the C-terminus of MYO3B (3B peptide). Error bars represent the standard deviation from three separate experiments.

Figure S2

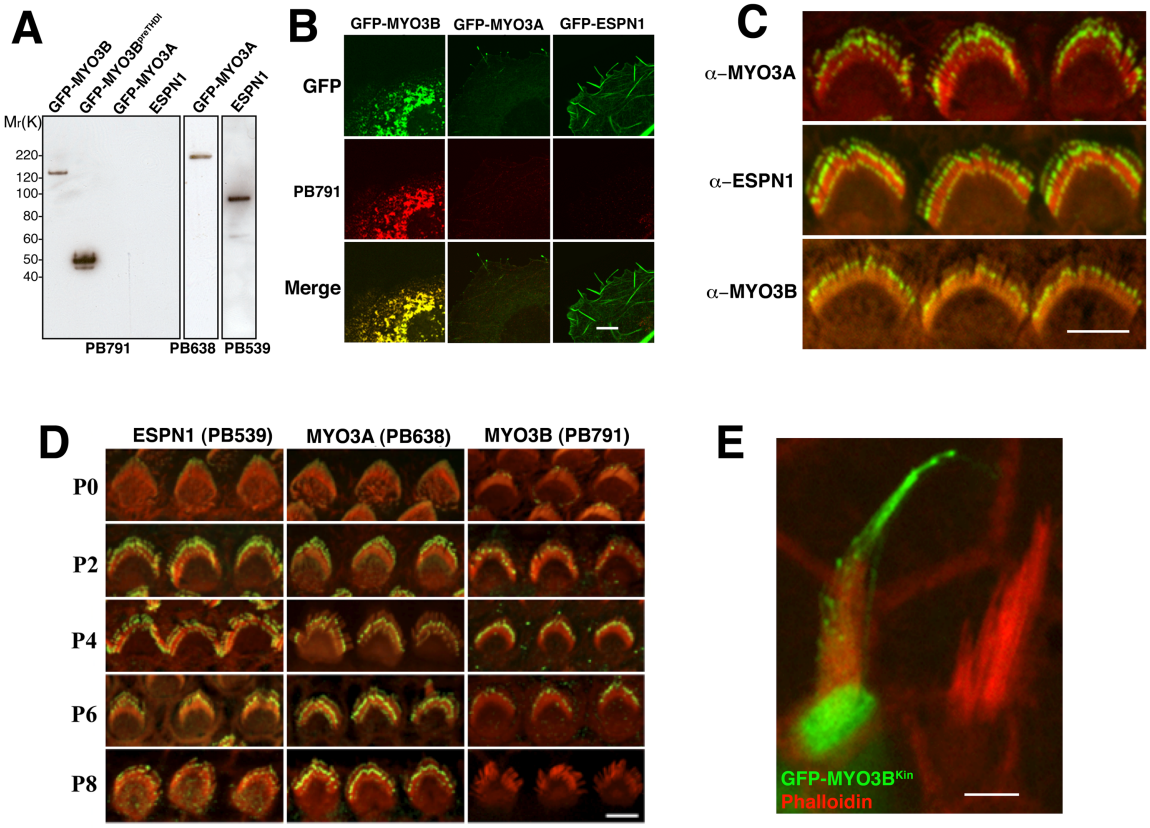


**Figure S2, related to Figure 2.** MYO3B localizes to the same compartment as MYO3A and ESPN1. (A) Immunoblots of COS7 cell lysates transfected with GFP-MYO3B, GFP-MYO3B$^{preTHDI}$, GFP-MYO3A, and ESPN1 show that PB791 specifically recognizes the tail of MYO3B but not MYO3A or ESPN1. (**B**) GFP-MYO3B (left column) overexpression in COS7 cells is recognized by PB791. The same antibody shows no labeling in COS7 cells with overexpressing GFP-MYO3A (middle column) or GFP-ESPN1 (right column). (C) Cochlear hair cells display MYO3B labeling at the tips of stereocilia, with higher amounts in the middle row, similar to MYO3A and ESPN1. Scale bar: 2 μm. (D) MYO3A and ESPN1 are strongly expressed at the tips of cochlear hair cell stereocilia from P0–P8, while MYO3B labeling is weak and diminishes to background levels by P8. Scale bar: 5 μm **(E)** A GFP-tagged MYO3B construct containing the N-terminus kinase domain (GFP-MYO3B$^{Kin}$) targets and elongates stereocilia tips. Scale bar: 5 μm.

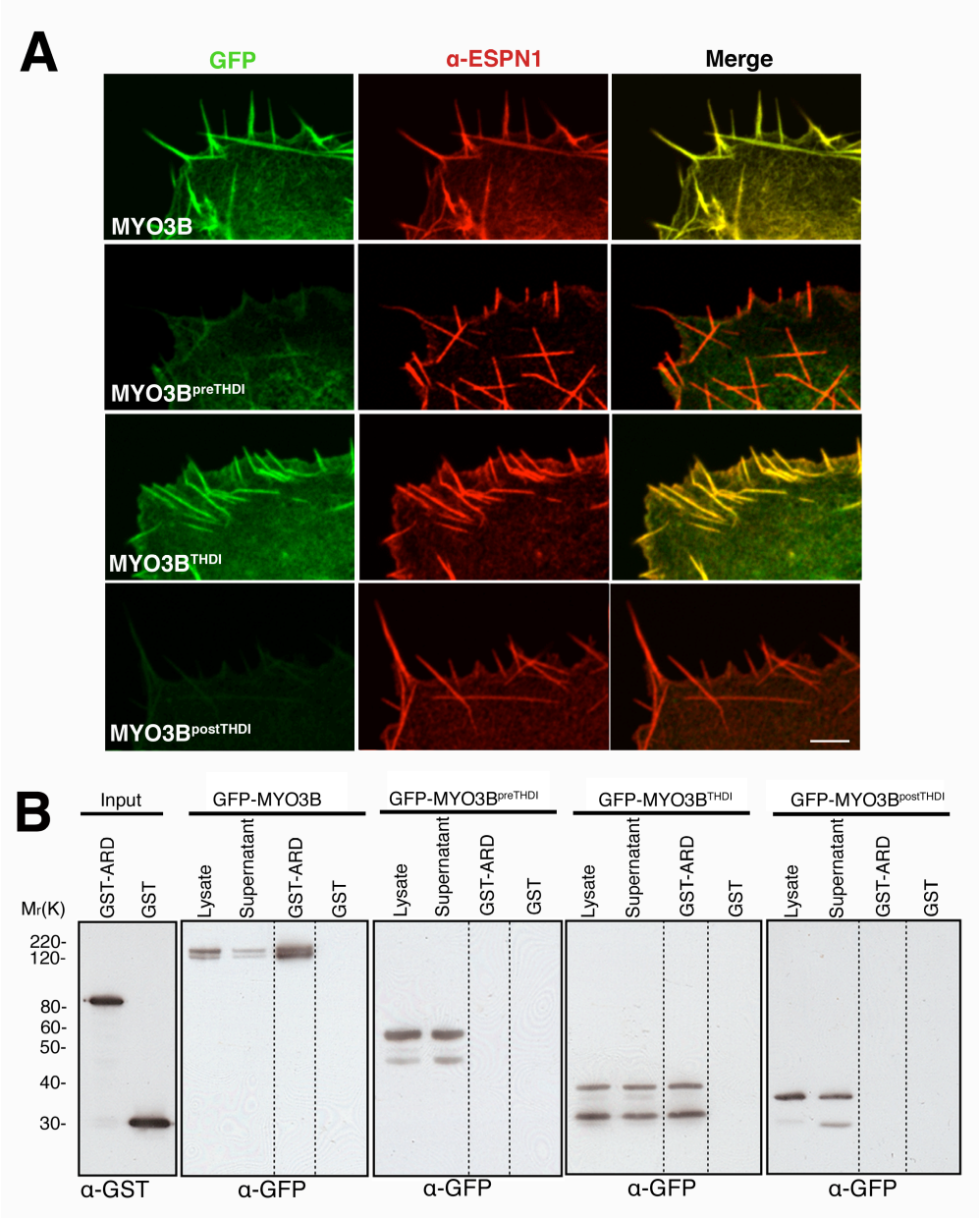


**Figure S3, related to Figure 3.** The MYO3B THDI interacts with the ESPN1 ARD in transfected COS7 cells and in vitro. (A) Co-expression of ESPN1 shows that GFP-MYO3B (first row; green) and GFP-MYO3B$^{THDI}$ (third row) colocalize with ESPN1 (red) in filopodia. Conversely, GFP-MYO3B$^{preTHDI}$ (second row), and GFP-MYO3B$^{postTHDI}$ (fourth row) appear diffuse throughout the cytoplasm, despite the presence of ESPN1 bundles. Scale bar: 1 μm. (B) GST pull-downs confirm that the THDI region of MYO3B is necessary for binding to ESPN1 ARD, as MYO3B$^{preTHDI}$ and MYO3B$^{postTHDI}$ show no binding to the ESPN1 ARD. Precipitates were detected using polyclonal α-GST and α-GFP antibodies.

**Table S1** Novel clones and associated primers used in this manuscript.

| DNA construct (aa) | Species (accession #) | Vector | Forward primer | Reverse primer |
|---|---|---|---|---|
| GFP-MYO3BΔTail (1-1141) | human (NM_138995) | pEGFP-C2 | 5′-GCTAGCGGCCGCCACC ATGCTTGGACTTGAATCACT TCCAGATCCCACAGACAC | 5′-GCCACATTCCCCCGTCGC AGCAGGTACGACTAGTGCTA |
| GFP-MYO3B$^{Kin}$ (1-1333) | mouse (BC156281) | pcDNA 6.2/N-EmGFP-DEST | n/a | n/a |
| GFP-MYO3B (303-1333) | | | 5′-GTTGCTAAAACCA GGCATGAAAGGATG | 5′-TCAGTGTTGAGCA AAGGGGTCTTCTC |
| GFP-MYO3B$^{TAIL}$ (909-1333) | | | 5′-GAGGCTCACATTC ACACAGTTCTCCA | |
| GFP-MYO3B$^{preTHDI}$ (1125-1248) | | | | 5′-TTATGCTCGCTGCT TCTGGGAGAGACCTTC |
| GFP-MYO3B$^{THDI}$ (1249-1306) | | | 5′- CCTCGCAGACGGTGT CAGCAGCCC AAAATG | 5′- TCACCCAGGGGACAGG CATTTGTAATACTGGTC |
| GFP-MYO3B$^{postTHDI}$ (1307-1333) | | | 5′-GCCTGTGCCC CTGAGGAAAC | 5′-TCAGTGTTGAGCA AAGGGGTCTTCTC |
| GFP-MYO3B$^{\Delta K-\Delta 23}$ (307-1310) | | pmCherry-C1 | 5′-ATGCTCCGGACCATTCA TTAAAGGAACTCAAGGC | 5′-ATGCAAGCTTAGGGGC ACAGGCCCCAGGGGAC |
| GFP-MYO3B$^{\Delta K-\Delta 23+3THDII}$ (mIIIb(307-1310) + hIIIa(1554-1616) | mouse (BC156281) + human (NM_017433) | | 5′-ATGCAAGCTTCATAGCCCT AGTTTAAGAGAACG | 5′-ATGCAAGCTTTTAGGACTG CTGGACGAGGCGCCGG |
| GFP-ESPN1ΔABM | human (NM_031475) | pcDNA 6.2/N-EmGFP-DEST | 5′- ATGGCCCTGGAGC AGGCGCTGCAG | 5′-TTACCGGACTGGTGACAGT GCAGGTGACACAGAAGGCA G |

## Materials and Methods

### Antibodies

Affinity-purified polyclonal rabbit antibody PB791 (Princeton Biomolecules) was generated against peptide (GESNRGHEETSRNC) corresponding to mouse MYO3B (GenBank: BC156281) amino acids 1155 to 1168. The antibodies specific for an N-terminal region conserved in mouse ESPN1 (PB539; [1]) and a C-terminal region in mouse MYO3A (PB638; [2]) have been previously described.

### Immunofluorescence and microscopy

Mice were sacrificed according to National Institutes of Health (NIH) guidelines under the National Institute on Deafness and other Communication Disorders animal protocol 1215-08, and their temporal bones perfused with 4% paraformaldehyde (PFA) in phosphate buffered saline (PBS; pH 7.4) through the round window and fixed for 30 min at room temperature. Inner ear epithelia were dissected in PBS, permeabilized with 0.5% Triton X100 for 30 min and blocked overnight at 4°C with filtered 4% bovine serum albumin (BSA) in PBS, and processed for immunofluorescence as previously described [3, 4]. Epithelia were then incubated with primary antibody for 2 hours, rinsed with PBS three times, stained with Alexa Fluor 488-conjugated secondary antibody (Molecular Probes) for 1 hour, rinsed with PBS three times, counterstained with Alexa Fluor-568 phalloidin (Molecular Probes), rinsed with PBS three times, and mounted using ProLong Gold antifade reagent (Invitrogen). Fluorescence confocal images were obtained with a Nikon microscope equipped with a 100X 1.45 numerical aperture (NA) objective and a spinning disk confocal unit (PerkinElmer).

**Expression plasmids**

All primers used for novel clones generated for this study are listed in Table S1. Full-length mouse MYO3B (NCBI accession number BC156281) in pENTR223.1 vector was obtained from Open Biosystems and the insert recombined with pcDNA 6.2/N-EmGFP-DEST vector by LR clonase using the Gateway Technology (Invitrogen). Full-length human MYO3B variant 2 (NM_138995) was obtained from Origene and the insert was subcloned by PCR and ligated to pCR8/GW/TOPO entry vector (Invitrogen). The insert was subsequently recombined with pcDNA 6.2/N-EmGFP-DEST vector by LR clonase. pcDNA3.1 expression vector containing inserts encoding for human ESPN1 wild-type and mutant WH2 (mWH2) domain have been described earlier. Constructs encoding MYO3B and ESPN1 deletion mutants (except GFP-MYO3BΔTail) were PCR subcloned into pCR8/GW/TOPO entry vector and recombined with pcDNA 6.2/N-EmGFP-DEST, pDEST-15 GST, and/or pcDNA/nV5-DEST expression vector by LR clonase. The GFP-MYO3BΔTail deletion mutant construct was directionally subcloned into the pEGFP-C expression vector (Clontech Takara, CA) in NotI and SpeI restriction sites. The chimeric pmCherry-MYO3B$^{\Delta K\text{-}\Delta 23+3THDII}$ (cherry-MYO3B:THDII) construct encoding for mouse MYO3B deleted of its N-terminal kinase domain and of its 23 C-terminal amino acids post-3THDI domain (aa 307-1310 of BC156281), and fused to human MYO3A 63 C-terminal amino acids (aa1554-1616 of NM_017433) corresponding to its 3THDII domain was generated in two steps. First, mouse MYO3B$^{\Delta K\text{-}\Delta 23}$ cDNA was amplified and directionally cloned into pmCherry-C1 BspEI and HindIII restriction sites, then 3THDII was cloned in tandem into HindIII site. All expression plasmids were

verified by sequencing, immunocytochemistry, and immunoblot.

**Cultures and transfection of COS7 cells**

COS7 cells (ATCC) were trypsinized, plated on coverslips and maintained at 37°C in DMEM supplemented with 10% fetal bovine serum (FBS). Cells were transfected using either GeneJuice (Novagen) or Lipofectamine transfection reagent (Invitrogen) according to manufacturer's instructions and incubated for 24 hours. Samples were then fixed for 20 min in 4% PFA in PBS, permeabilized for 30 min in 0.5% Triton X-100 in PBS, and counterstained or processed for immunofluorescence as described earlier.

**Live-cell analysis of MYO3A and MYO3B movements in ESPN1-expressing cells via TIRF microscopy.**

Intracellular movements of GFP-labeled MYO3 constructs were imaged in living cells using a method similar to [5] with some modifications. COS7 cells were grown in DMEM supplemented with 10% FBS and antibiotics on 22mm, #1.5 coverslips overnight, and then transfected using Fugene HD (Roche) with low amounts of unlabeled ESPN1 (0.1mg DNA/coverslip) and GFP-MYO3A (0.3mg/coverlsip) or GFP-MYO3B (0.3mg/coverslip) and allowed to express the protein for approximately 16 hours. Transfected coverslips were then mounted in Rose chambers with a 3mm foam spacer and a coverslip roof; the chamber was filled with Optimem supplemented with antibiotics. Objective-type TIRF imaging was performed using a Nikon TE2000-PFS equipped with a TIRF-II illuminator and a 60x/1.49NA objective. TIRF-illumination was provided by a 300 mW argon laser (set to ~30mW at 488nm) and an AOTF was used for rapid wavelength

selection and shuttering. Images were captured through a Chroma #41001 filter cube using a Photometrics Coolsnap HQ2 cooled-CCD camera. All hardware components and image acquisition were controlled using mHQ2 cooled-CCD came [6]. To determine the velocities of moving features, kymographs were generated from the time-lapse images using Metamorph 6.0 (Molecular Devices), and tracks of moving fluorescent puncta were identified manually.

**Culture and transfection of rat inner ear tissue**

Organ of Corti and vestibular tissues were dissected from postnatal day 0–8 rats and attached to CellTak (BD Biosciences) -coated coverslips. Cultures were maintained in DMEM/F12 (Invitrogen) with 5–7% FBS and ampicillin (1.5 μg ml–1; Sigma) and kept at 37°C and 5% $CO_2$. For transfections, 50 μg of DNA were precipitated onto 25 mg of 1 μm gold particles and loaded into the Helios Gene Gun cartridges (BioRad). Tissue explants were transfected with the gene gun set at 95 psi of helium and maintained in culture for 18–48 hours. Samples were fixed and counterstained for confocal microscope viewing as described above. The efficiency of transfection ranged from 0–9 hair cells per explant.

**Image Analysis and Quantification**

Physical quantities of stereocilia and filopodia were measured using confocal microscopy and NIH ImageJ. Relative pixel intensity of protein fluorescence was quantified by the difference in the fluorescence intensity between a region over the stereocilia bundle and an arbitrary background region [7] divided by the fluorescence intensity of phalloidin (red). All relative pixel intensity numbers were normalized.

To estimate the relative increase in stereocilia length, we compared the heights of the tallest row of well-preserved stereocilia of transfected CHCs and VHCs ($H_T$) with the average height of all their respective neighboring (usually between 3 to 5) non-transfected cells ($H_{NT}$), within the field of view of our camera/confocal setup (30 × 45 µm). The average ratio of stereocilia length *RL* was calculated as $RL = \frac{H_T}{H_{NT}}$. All ANOVA tests were performed using MATLAB (Mathworks).

Measurements of average filopodia lengths of transfected COS7 cells were performed using NIH ImageJ by measuring the distance from the periphery of the cell to the filopodia tip.

The half-length $L_h$ was calculated as the ratio $L_h = \frac{L_{1/2}}{L_{min}}$, where $L_{1/2}$ is the measured distance from the tip of the filopodia to where the fluorescence intensity was at half-maximum, and $L_{min}$ is the distance from the tip of the filopodia to where the fluorescence intensity reached a minimum.

**Western blotting**

100-mm dishes of transfected semi-confluent COS7 cells were rinsed in PBS and scraped in 300 µl of ice-cold cell lysis buffer (CLB): $dH_2O$, 1% Triton X-100, 5 mM dithiothreitol, 150 mM NaCl, 50 mM Tris, 2 mM EDTA, 1 mM Pefabloc, 1x Pefabloc protector, and 1% mammalian protease inhibitor cocktail (Sigma). After addition of 1× loading sample buffer (Invitrogen), samples were boiled and sample reducing agent (Invitrogen) added. 10 µl of lysates were loaded in NuPAGE 4–12% Bis-Tris mini-gel (Invitrogen). Western blots were blocked

overnight at 4°C with 5% nonfat milk (Bio-Rad, Hercules, CA) and incubated with primary antibody for 2 hours. Horseradish peroxidase-conjugated goat anti-rabbit antibodies (Santa Cruz) and ECL chemiluminescence system (Amersham Biosciences) were used for detection.

**GST pulldown assays**

Protein expressions of glutathione S transferase (GST) alone or fused to ARD (GST–ESPN1$^{ARD}$) and protein purification are previously described (1). Briefly, GST proteins were isolated from bacterial lysates using glutathione–Sepharose 4B beads (Amersham Biosciences). GFP–MYO3B$^{\Delta K}$, –pre3THDI, –3THDI and –post3THDI fusion proteins were extracted from 24-hour transfected COS7 cells by brief sonication in ice-cold CLB and 30min ultracentrifugation at 145,000 g. To test for MYO3B interactions, the same amount of GST–ESPN1$^{ARD}$ or GST alone was bound to 4B beads for 1 hour at 4°C followed by incubation with the same amount of a GFP-tagged MYO3B fragment in CLB for 1.5 hours. The beads were then washed three times with CLB. 10 µl of co-precipitates were loaded, separated by electrophoresis on NuPAGE Bis-Tris 4–12% gels, and analyzed by Western blotting using rabbit polyclonal anti-GFP and anti-GST antibodies (Invitrogen).

**ATPase, ADP release, and kinase activity of MYO3B 2IQ.**

Recombinant MYO3B 2IQ (residues 1-1143) with a C-terminal FLAG tag (DYKDDDDK) was expressed in the baculovirus SF9 insect cell system and purified with anti-FLAG affinity chromotagraphy, as was performed with MYO3A

2IQ [8-10]. The NADH-coupled ATPase assay was used to examine MYO3B 2IQ actin-activated ATPase activity [8-10]. The ATPase assays were performed with 0.1 mM MYO3B 2IQ and a range of actin concentrations (0, 5, 10, 20, 40, and 60 mM) in an Applied Photophysics (Surrey, UK) stopped flow device. The ATPase rates were plotted as a function of actin concentration and fit to Michaelis-Menten kinetics to determine the maximal actin-activated ATPase rate ($k_{cat}$) and actin concentration at which one-half maximal ATPase was achieved ($K_{ATPase}$) [8-10]. The rate of ADP-release from the motor catalytic site of MYO3B 2IQ was examined by stopped flow mixing experiments. An equilibrium mixture of acto-MYO3B 2IQ in the presence of ADP was mixed with saturating ATP (final concentrations: 0.6 μM actin, 0.5 μM MYO3B 2IQ, 5 μM ADP, and 2.5 mM ATP). We monitored the decrease in light scatter observed upon the dissociation of myosin from actin, which is limited by the release of ADP prior to ATP binding under these conditions [6]. The kinase activity of MYO3B 2IQ was measured with $^{32}$P ATP assays as described [8, 10].

**MYO3 Tail Binding Assays.**

Examination of GST 3THDII fusion proteins (described above), a peptide of the 3THDII region of MYO3A (amino acids 1588-1616), and a peptide corresponding to the C-terminus of bass MYO3B (amino acids 1293-1310) were performed by measuring pyrene actin quenching as described [8, 9]. Equilibrium measurements were made by measuring the degree of pyrene quenching in the presence and absence of GST only, GST 3THDII, 3THDII peptide, or 3B peptide

in a Quantamaster fluorometer (Photon Technology International, Lawarenceville, NJ) with an excitation of 365 nm and scanning the fluorescence emission between 380-500 nm. The data was fit to a hyperbolic binding equation to determine the affinity of the tail constructs for actin. Transient kinetic measurements were performed in the stopped flow [8, 9] keeping the GST 3THDII concentration at least 5-fold less than the pyrene actin concentration. The fluorescence transients were fit with custom software provided by Applied Photophysics and errors are reported as standard error of the fits.


1. Salles, F.T., Merritt, R.C., Jr., Manor, U., Dougherty, G.W., Sousa, A.D., Moore, J.E., Yengo, C.M., Dose, A.C., and Kachar, B. (2009). Myosin IIIa boosts elongation of stereocilia by transporting espin 1 to the plus ends of actin filaments. Nature cell biology *11*, 443-450.
2. Schneider, M.E., Dose, A.C., Salles, F.T., Chang, W., Erickson, F.L., Burnside, B., and Kachar, B. (2006). A new compartment at stereocilia tips defined by spatial and temporal patterns of myosin IIIa expression. J Neurosci *26*, 10243-10252.
3. Rzadzinska, A.K., Schneider, M.E., Davies, C., Riordan, G.P., and Kachar, B. (2004). An actin molecular treadmill and myosins maintain stereocilia functional architecture and self-renewal. The Journal of cell biology *164*, 887-897.
4. Grati, M., Schneider, M.E., Lipkow, K., Strehler, E.E., Wenthold, R.J., and Kachar, B. (2006). Rapid turnover of stereocilia membrane proteins: evidence from the trafficking and mobility of plasma membrane Ca(2+)-ATPase 2. J Neurosci *26*, 6386-6395.
5. Kerber, M.L., Jacobs, D.T., Campagnola, L., Dunn, B.D., Yin, T., Sousa, A.D., Quintero, O.A., and Cheney, R.E. (2009). A novel form of motility in filopodia revealed by imaging myosin-X at the single-molecule level. Curr Biol *19*, 967-973.
6. Edelstein, A., Amodaj, N., Hoover, K., Vale, R., and Stuurman, N. (2010). Computer control of microscopes using microManager. Curr Protoc Mol Biol *Chapter 14*, Unit14 20.
7. Waguespack, J., Salles, F.T., Kachar, B., and Ricci, A.J. (2007). Stepwise morphological and functional maturation of mechanotransduction in rat outer hair cells. J Neurosci *27*, 13890-13902.

8. Dose, A.C., Ananthanarayanan, S., Moore, J.E., Burnside, B., and Yengo, C.M. (2007). Kinetic mechanism of human myosin IIIA. The Journal of biological chemistry *282*, 216-231.
9. Dose, A.C., Ananthanarayanan, S., Moore, J.E., Corsa, A.C., Burnside, B., and Yengo, C.M. (2008). The kinase domain alters the kinetic properties of the myosin IIIA motor. Biochemistry *47*, 2485-2496.
10. Quintero, O.A., Moore, J.E., Unrath, W.C., Manor, U., Salles, F.T., Grati, M., Kachar, B., and Yengo, C.M. (2010). Intermolecular autophosphorylation regulates myosin IIIa activity and localization in parallel actin bundles. The Journal of biological chemistry *285*, 35770-35782.